Pulsed Laser Powered Homogeneous Pyrolysis for Reaction Kinetics Studies: Probe Laser Measurement of Reaction Time and Temperature

MARK T. SWIHART and ROBERT W. CARR

Department of Chemical Engineering and Materials Science, University of Minnesota, 421 Washington Ave. SE, Minneapolis, Minnesota 55455

ABSTRACT

Pulsed laser powered homogeneous pyrolysis (LPHP) is a technique which can be used to measure rate parameters for purely homogeneous unimolecular decomposition reactions at high temperatures (600–1500 K). The reaction temperature in pulsed LPHP may be obtained from the speed of sound in the reacting gas, which may be measured by observing the thermal lens effect of the gas on a probe laser beam. The reaction time may be obtained directly from the thermal lens measurements. In this work experiments were performed using ethyl acetate (EtAc) and isopropyl chloride (2-ClPr), two reactants whose unimolecular decomposition rate parameters are well established. This allowed us to assess the accuracy and precision attainable with this technique. Pulsed LPHP proved capable of providing rate parameters in good agreement with those in the literature. The results for which the measured activation energies were closest to the literature values gave the temperature dependence of the rate constants as $\log(k_{EtAc}) = (12.0 \pm 0.9) - 47.7 \pm 4.4$(kcal/mol)/2.303RT and $\log(k_{2\text{-ClPr}}) = (13.3 \pm 1.0) - 50.8 \pm 4.8$(kcal/mol)/2.303RT. These may be compared with the literature recommendations, $\log(k_{EtAc}) = 12.6 - 48.0$(kcal/mol)/2.303RT and $\log(k_{2\text{-ClPr}}) = 13.6 - 51.1$(kcal/mol)/2.303RT. In all cases the measured rate parameters agreed with the recommended values to within the error limits of the measured values. Potential sources of error in the temperature measurement and the kinetic parameters are explored. The expected accuracy of the experiments is assessed, and possible improvements in the experiment are suggested. © 1996 John Wiley & Sons, Inc.

Received January 2, 1996; accepted April 19, 1996
International Journal of Chemical Kinetics, Vol. 28, 817–828 (1996)
 CCC 0538-8066/96/110817-12

INTRODUCTION

Although a number of researchers have shown that pulsed laser powered homogeneous pyrolysis (LPHP) can be used for measuring bond energies and rate pa-

rameters for homogeneous unimolecular decomposition reactions [1–5], the LPHP technique has not been widely used for the study of these reactions. Since it has seen less use, the LPHP technique is somewhat less developed than the single pulse shock tube, the dominant technique used for high temperature kinetics. However, with some refinement, LPHP has the potential to become a routine and reliable method, playing a role complementary to shock tube studies. LPHP is applicable at slightly lower temperatures and pressures than are ordinarily used in shock tube experiments. Lack of use of LPHP has been at least partially due to the difficulty of making measurements of the reaction time and temperature in pulsed LPHP. This article presents results obtained using a probe laser to monitor the reaction time and temperature by observing the thermal lens effect of the gas in the reactor on the probe laser. This time and temperature determination can be used alone or in conjunction with comparative rate techniques similar to those used in many shock tube experiments.

A particular field in which LPHP could play an important role is in providing rate parameters important in modeling chemical vapor deposition (CVD) reactors used in the manufacture of microelectronics. The gas-phase chemistry in many CVD systems is strongly influenced by the unimolecular decomposition of a precursor species. Examples of this include dichlorosilane decomposition in CVD of epitaxial silicon [6,7], trimethylgallium decomposition in MOCVD of GaAs [8], and silane decomposition in CVD of polycrystalline silicon [9,10]. Further advances in CVD technology, such as improvements in film uniformity, more precise control of film properties, and increases in wafer size, will depend on the development of quantitative, predictive, physically based mathematical models of CVD processes. Accurate values of rate parameters for the gas-phase unimolecular decomposition of precursor molecules are critical ingredients in these models. Obtaining these rate parameters is complicated by the fact that the organometallic precursor molecules react on hot surfaces as well as in the gas phase. Thus, the rate constants need to be measured in a reactor with no hot walls. Pulsed LPHP is a technique which can provide a reactor without hot walls, and which can be used to measure rates of unimolecular decomposition reactions over the range of temperatures commonly used in CVD processes.

In pulsed LPHP, an infrared laser is used to rapidly heat a column of gas to 600–1500 K, inducing reaction. If the laser beam does not fill the entire reactor, this gas then expands and cools, quenching the reaction in a time on the order of 10 μs. The reactor walls remain at room temperature. In order to make chemical kinetic measurements, the reaction time and reaction temperature must be determined. One way to do this is through comparative rate techniques, in which the rate parameters for the species being investigated are obtained by comparison to another reactant whose rate parameters are known [1–5]. This method is effective when a compound with well known rate parameters which are close to those of the reactant of interest is available, and when this compound reacts independently of the reactant being investigated.

An alternate means of determining the reaction time and temperature uses the time dependent thermal lensing effect [11,12]. In this technique, a probe laser is combined coaxially with the infrared beam that heats the reaction mixture. A pinhole is placed on the axis of the probe beam, some distance past the reactor. The amount of light passing through the pinhole is monitored. After the infrared laser pulse, the heated gas expands, creating a transient, nonuniform density profile. This nonuniform density profile leads to a nonuniform profile of refractive index, which acts as a lens, focusing or defocusing the probe beam [13,14]. It is known that the expansion of the heated column of gas takes place via the passage of a rarefaction wave, which moves at the speed of sound in the heated region [11,12,15]. When this wave reaches the axis of the heated region, it creates a nonuniform density profile in which the gas density is highest on the beam axis. At the pressures used in these experiments, the refractive index is approximately proportional to the gas density [13]. So, when the expansion wave reaches the beam axis, a nonuniform profile of refractive index is created in which the refractive index is a maximum on the beam axis. This acts as a converging lens, focusing the probe beam onto the pinhole. This causes a peak (a maximum) in the thermal lens signal, the measured amount of light passing through the pinhole. The time between the firing of the laser and the appearance of this peak in the thermal lens signal is the time required for the expansion wave to traverse the beam radius. This is also the reaction time. Dividing the beam radius by this delay time gives us the speed of sound in the heated gas. Through the temperature dependence of the speed of sound, we may then determine the temperature in the heated column of gas. A more detailed discussion of the gas dynamics following a laser pulse may be found in ref. [15].

This article presents the results of experiments designed to assess the accuracy of chemical kinetic measurements made using the pulsed LPHP technique with temperature measurement from the thermal lens effect, as described above. Experiments

were performed using a pair of compounds whose rate parameters are well known, so that measurements could be compared to results in the literature. Computational simulations of the experiment have also been performed to investigate the effect of known potential sources of systematic error in the experiment and associated data analysis.

EXPERIMENTAL

The experimental arrangement used for the pulsed LPHP experiments is shown schematically in Figure 1. A Lumonics model TEA 101-2 pulsed CO_2 laser was used to heat the reaction mixture. The spatial energy profile of the portion of the beam used was nearly uniform in the horizontal direction, but decreased moving away from the beam axis in the vertical direction. At 0.32 cm above or below the beam axis, the energy was about 85% of its value on the beam axis. Typical laser fluence was 1.2 J/cm^2. The laser was tuned to the P(16) line of the 00^01-10^00 band. with a wavelength of 10.55 μm. The infrared beam was combined coaxially with the beam from a Uniphase model 1101 HeNe laser (diameter = 0.63 mm) using a coated germanium flat. The combined beams were passed through an orifice which defined the diameter of the infrared beam, then through the reaction cell. The reaction cells were constructed from 1 inch OD pyrex tubing with NaCl windows (5 mm thick) on the ends. Two different reaction cells were used in these experiments. The longer cell had a volume of 11.7 cm^3 and a length of 3.05 cm between the windows. The shorter cell had a volume of 4.83 cm^3 and a length of 0.85 cm. After passing through the reactor, the two laser beams were separated, using another germanium flat. The CO_2 beam impinged on a Rofin model 7425 photon drag detector. A pinhole (350 μm diameter) was placed on the axis of the HeNe beam. This was followed by a diverging lens, a 633 nm band pass filter, and a photomultiplier tube (RCA 1P28). The signal from the photomultiplier tube was passed through a current-to-voltage amplifier and displayed on a Tektronix model 2230 100 MHz digital storage oscilloscope. The rise time of the detection electronics was under 0.1 μs. The signal from the photon drag detector, which corresponded to the temporal profile of the CO_2 laser pulse, was used to trigger the oscilloscope on the leading edge of the laser pulse.

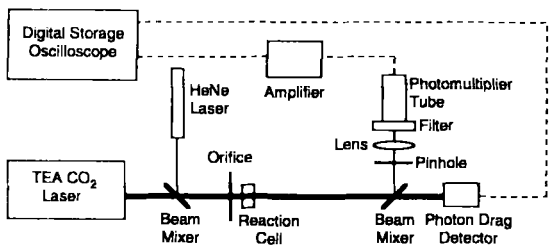

Figure 1 Schematic diagram of the experimental layout.

Experiments were carried out using ethyl acetate (EtAc) (Mallinckrodt, 99.9%) and isopropyl chloride (2-chloropropane (2-ClPr), Aldrich, 99+%) as reactants. Sulfur hexafluoride (Matheson, CP grade) was used as the photosensitizer, absorbing the 10.55 μm radiation and transferring the energy to the other species via collisions. Nitrogen (Air Products, ultrahigh purity grade) was used as the bath gas. The composition of a typical reaction mixture was 0.6–1% each of EtAc and 2-ClPr, 6–11% SF_6, and the balance N_2. Mixtures of EtAc, 2-ClPr, and SF_6 were prepared manometrically and stored in a two liter glass bulb on a vacuum line which could be evacuated to below 10^{-5} torr. A few torr of this mixture was added to the reaction cell, then N_2 was added to reach the desired reaction pressure (typically 100 torr). The reaction temperature was varied by using more or less of the mixture containing the reactants and photosensitizer. More photosensitizer led to stronger absorption of the CO_2 laser beam and higher temperatures.

The reaction cell was mounted so that its front window nearly touched the orifice which defined the infrared beam diameter. This minimized effects of diffraction of the CO_2 beam by the orifice. The cell was aligned so that its windows were perpendicular to the laser beams, and so that the beams passed through the cell in an off-axis position. It is important that the beams not be on the axis of the reaction cell, because this can result in constructive interference of shock waves reflected from the reactor walls, which will reheat the gas mixture and cause additional reaction [7]. Precise positioning of the portion of the CO_2 beam used, such that the HeNe beam and pinhole were on its axis, was accomplished by moving the orifice which defined the CO_2 beam. Its position was adjusted so that the peak in the observed thermal lens signal was as tall and narrow as possible. The shape and location of the peak in the thermal lens signal were insensitive to changes in the alignment over a range of about 150 μm.

An experiment consisted of between 750 and 4500 laser pulses, at a repetition rate of about 0.35 Hz. The low repetition rate was necessary both for smooth operation of the laser and to allow the reaction cell contents to mix thoroughly and cool back to room temperature between pulses. It was found that the laser

energy decreased significantly during the first hour of operation, so all experiments were conducted after allowing the laser to warm up for at least 1 h. A 0.635 cm diameter portion of the CO_2 beam was used in these experiments. The thermal lens signal after each pulse was averaged into the existing signal from previous pulses stored on the oscilloscope. After 150 pulses the delay time (t_r) from the averaged signal was recorded, and the averaging process started over. This was necessary to take into account slight changes in the laser energy over the course of the experiment which resulted in slight changes in the measured delay time and the temperature computed from it.

The two reactions under consideration were:

$$CH_3CHClCH_3 \longrightarrow CH_2CHCH_3 + HCl \quad (1)$$

$$\text{and } CH_3COOC_2H_5 \longrightarrow C_2H_4 + CH_3COOH \quad (2)$$

Both reactions have been widely studied, and side reactions have not been observed. The products do not undergo significant further decomposition or reaction at the reaction times and temperatures used. Rate parameters for these reactions have been measured using several techniques, and the results agree well ([16–20] for 2-ClPr, [21–26] for EtAc). The rate parameters recommended by Benson and O'Neal [27] are shown in Table I. These are consistent with more recent measurements. Comparing the results from different researchers, it appears that for both reactions uncertainty in the activation energy is around 0.5 kcal/mol and uncertainty in log(A) is around 0.2. RRK calculations, along with low pressure data from [16] and [23], allow us to conclude that fall-off effects are not significant for either reaction at the temperatures and pressures used in these experiments.

The reaction products were analyzed on a Varian model 3700 gas chromatograph equipped with a flame ionization detector. A 6 ft. column packed with Porapak QS was used at 170°C. The reaction products measured and quantified were ethene (from reaction (2)) and propene (from reaction (1)). The HCl produced by reaction (1) cannot be detected by the flame ionization detector. The acetic acid produced by reaction (2) had a much longer retention time than the other species present and eluted as a small, broad peak which was not readily quantified. No other products were detected by GC analysis. Reactant conversions were calculated based on measured product and reactant areas, adjusting for the differing response of the flame ionization detector to the different species. Fractional conversion of the reactants ranged from about 0.5% to 40%, depending on the temperature and number of laser pulses used.

DATA ANALYSIS AND MODELING

As shown in ref. [15], a simple analysis of the wave propagation process leads to the following expression for the rate constant:

$$k\,t_r = 3\,(V_T/V_l)\,(1 - (1 - x)^{(1/n)}) \quad (3)$$

where x = measured reactant conversion, V_T = total reactor volume, V_l = volume irradiated by infrared beam, n = number of laser pulses, and t_r = reaction time. In this work t_r was measured by the thermal lens technique. As also discussed in ref. [15], the rate constant from this simple analysis must be corrected to account for reaction which occurs behind the head of the rarefaction wave. The correlation for making this adjustment that was presented there was used in this work. The correlation represented detailed simulation results to within 1–2%. The correction factor was between 0.75 and 0.80 for most of the data presented here.

The speed of sound in the reacting gas was obtained by dividing the known beam radius (taken from the diameter of the orifice used to define it) by the measured time from the laser firing to the peak in

Table I Values of Rate Parameters

	EtAc Decomposition		2-ClPr Decomposition	
Method	E_a kcal/mole	log(A)	E_a kcal/mole	log(A)
Recommended Values [27]	48.0	12.6	51.1	13.6
Comparative Rate, Long Reactor	48.9 ± 1.2	12.6 ± 0.3	50.0 ± 1.2	13.6 ± 0.3
Comparative Rate, Short Reactor	48.0 ± 1.1	12.4 ± 0.3	51.0 ± 1.2	13.8 ± 0.3
Thermal Lensing, Long Reactor	50.4 ± 4.0	12.9 ± 0.9	52.5 ± 3.8	13.9 ± 0.8
Thermal Lensing, Short Reactor	44.5 ± 4.0	12.1 ± 0.9	47.4 ± 4.4	13.3 ± 1.0
Thermal Lensing, Short Reactor, After Adjusting t_r	47.7 ± 4.4	12.0 ± 0.9	50.8 ± 4.8	13.3 ± 1.0

the thermal lens signal. The temperature was obtained from the speed of sound in the gas according to:

$$T = (a^2M)/(\gamma R) \quad (4)$$

where T = temperature, a = speed of sound, M = average molecular weight, R = universal gas constant, and γ = the specific heat ratio (C_p/C_v). Since γ is temperature dependent, this required a simple iterative process to find the temperature. Polynomial fits to the specific heats of the gases were obtained from data in the literature [28,29] and were used to calculate γ.

The equations which govern the gas dynamics and chemical reaction after a laser pulse were presented in ref. [15]. The solution method and computer program discussed there have been extended to allow simulations in two dimensions in a plane perpendicular to the reactor axis. This allows computational investigation of effects of heating which is nonuniform in this plane. The simulations also provide computed thermal lens signals which can be used to see the effects on nonidealities in the experiment on the resulting thermal lens signal, and hence the measured temperature.

RESULTS

Thermal Lens Measurements

Figure 2 shows a typical thermal lens signal obtained with the 0.635 cm diameter orifice defining the CO_2 beam. The peak (maximum voltage) in the signal corresponds to the arrival of the head of the rarefaction wave at the beam axis. The reaction time (t_r) was measured from the trigger position to the highest point of the peak. The trigger position corresponds to the beginning of the steep front edge of the temporal profile of the CO_2 laser pulse. Since the total rise time of the front edge of the laser pulse is only about 50 ns, the exact position on this edge is not critical. The approximately 0.6 μs rise time of the peak in the thermal lens signal is roughly equal to the time required for the head of the rarefaction wave to traverse the radius of the HeNe beam. However, it is not clear that these times are directly related. The width of the pulse may also be associated with noninstantaneous and nonuniform heating of the gas in the reactor. The shape of the signal was independent of the total pressure, beam diameter, gas composition, and cell length. The height of the peak increased with decreasing beam diameter, increasing pressure, and increasing cell length.

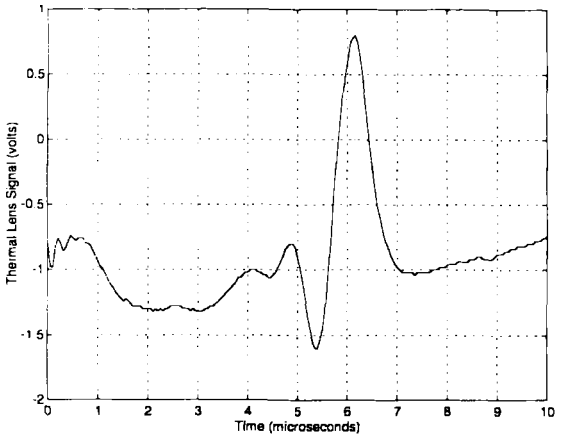

Figure 2 A typical thermal lens signal. This is for a mixture of 0.86 torr 2-ClPr, 0.96 torr EtAc, 10.08 torr SF_6, and 89.1 torr N_2 in the long reaction cell.

Figure 3 shows plots of the measured delay time vs. the beam radius for typical gas mixtures in the long (Fig. 3(a)) and short (Fig. 3(b)) reaction cells. Note that the plots are almost perfectly linear, providing partial confirmation that our interpretation of the gas dynamics and the thermal lens signal is correct. The slope of this line is the inverse of the speed of sound in the mixture. For the long reaction cell (Fig. 3(a)) the y-intercept of the best fit line is nearly zero. Its mean value from 5 experiments was 0.016 μs, with individual values ranging from -0.02 to 0.07 μs. A y-intercept of zero would be expected based on our interpretation of the measured delay time. For the short reaction cell, the y-intercept is significantly different from zero. In five experiments it ranged from 0.17 to 0.30 μs with a mean value of 0.222 μs. Possible reasons for this nonzero value are presented below.

Kinetics by Relative Rate Method

Figure 4 shows plots of $\log(k_{EtAc}t_r)$ vs. $\log(k_{2\text{-ClPr}}t_r)$. This is essentially the standard comparative rate technique. One reaction is chosen as the reference, and rate parameters for the other reaction are determined from the relative rate plot. The equation relating the rate constants and reaction time is [2,30]:

$$\log(k_1t_r) = \log(A_1) - (1 - E_1/E_2)\log(t_r) - E_1/E_2\log(A_2) + E_1/E_2\log(k_2t_r) \quad (5)$$

Thus, the slope of the plot gives the ratio of the activation energies of the reactions. The value of $E_{a,EtAc}/E_{a,2\text{-ClPr}}$ obtained from the literature is 0.94. The best fit to the data from the long reactor (Fig.

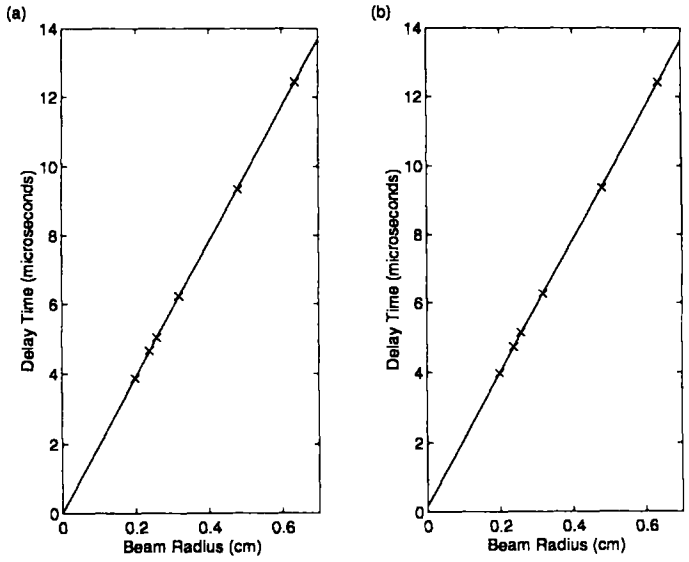

Figure 3 Plots of the measured delay time (the time between laser firing and the peak in the thermal lens signal) vs. the radius of the laser beam. (a) Typical results from the long (3.05 cm) reactor and (b) typical results from the short (0.85 cm) reactor.

4(a)) has a slope of 0.96 ± 0.02. The best fit to the short reactor data has a slope of 0.94 ± 0.02. Stated error limits are calculated using twice the calculated standard deviation of the slope and intercept of the comparative rate plots. These results reaffirm that the comparative rate technique works well when a good thermal monitor molecule is available.

To obtain preexponential factors from (5) one must assume that the reaction time (t_r) is the same for all of the data points and measure or guess a value for it. However, if the thermal lens technique is used to measure the reaction time for each data point, then one can plot the rate constants themselves, rather than the rate constant-reaction time products used in the standard comparative rate technique. Figure 5 shows plots of $\log(k_{\text{EtAc}})$ vs. $\log(k_{\text{2-ClPr}})$, where the rate con-

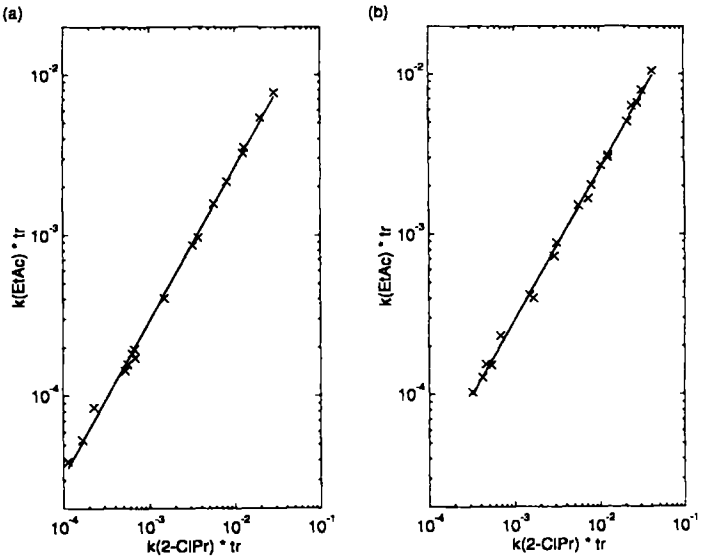

Figure 4 Standard comparative rate plots, see eq. (5). (a) Results from long reactor and (b) results from short reactor. The solid line is the best fit to the data.

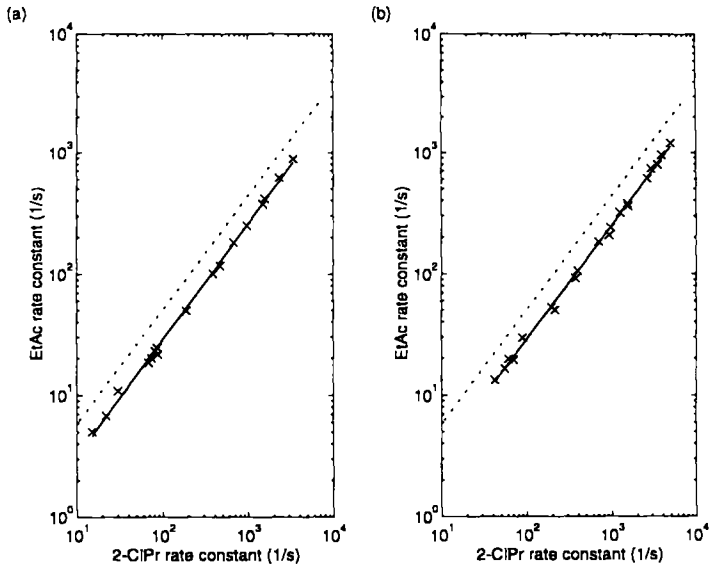

Figure 5 Modified comparative rate plots, see eq. (6). (a) Results from long reactor and (b) results from short reactor. The solid line is the best fit to the data. The dashed line is from the literature values for the rate constants.

stants have been calculated according to (1) with t_r from the thermal lens measurements. The relationship between the rate constants is

$$\log(k_1) = (A_1) - E_1/E_2\log(A_2) + E_1/E_2\log(k_2) \quad (6)$$

As with the standard comparative rate expression, the slope of the plot is the ratio of activation energies, but now the intercept of the plot gives a relationship between the preexponential factors of the reactions as well. The use of the thermal lens measurements of the reaction time therefore makes it possible to obtain good measurements of the preexponential factor from the comparative rate technique. The values of the rate parameters obtained for each reaction by using the other reaction as the reference are given in Table I. These results agree very well with the literature values of the rate parameters. The error estimates could be reduced further by the addition of more data points.

Kinetics from Thermal Lensing

Figures 6(a) and 6(b) show Arrhenius plots for 2-ClPr decomposition and EtAc decomposition in the long and short reactors, respectively, with the reaction time and temperature obtained from the thermal lens signals. The rate parameters from the best fits to the data are shown in Table I. Note the good agreement between the literature values and the results from the long reactor presented in Figure 6(a). Again, the stated error limits in Table I are two standard deviations computed from the scatter in the data, and are therefore generous. The error limits could be reduced somewhat by the addition of more data points. The activation energies measured in the short reaction cell are lower than both the literature values and the values measured in the long reaction cell, but the literature values do lie within the error limits of the measured values. In determining the parameters stated above, a least-squares fitting procedure was used that minimized the error in $1/T$ rather than minimizing the error in $\log(k)$. This is appropriate because the bulk of the uncertainty in the measurements is in the temperature measurement, rather than in the rate constant measurement. Fitting the data to minimize error in $\log(k)$ gave activation energies which were 1 to 2 kcal/mol lower.

DISCUSSION

Nonzero Intercepts in Delay Time vs. Beam Radius Plot

It was observed above that the plot of the measured delay time vs. the radius of the CO_2 laser beam for the short reaction cell did not pass through the origin, contrary to expectations. There are several possible reasons for this. The two which appear to be most significant are discussed here. First, the duration of the laser pulse which heated the reaction mixture was a significant fraction of the reaction time. The tempo-

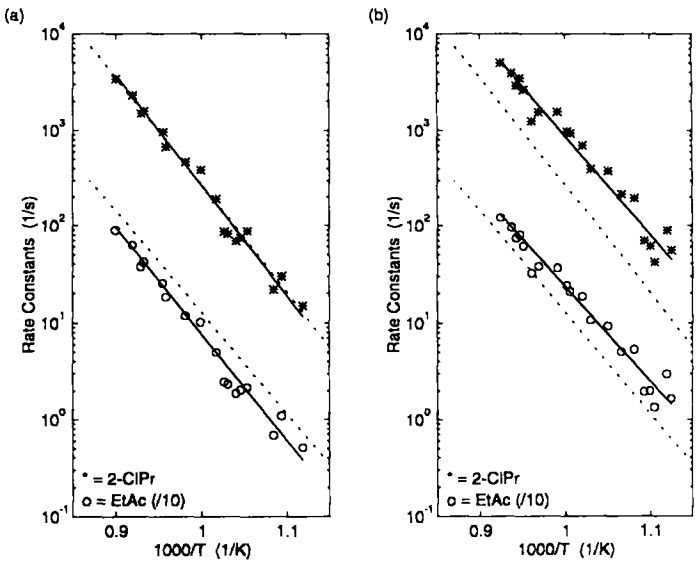

Figure 6 Arrhenius plots of the data with temperatures from the thermal lens measurements. Note that the rate constants for EtAc decomposition have been divided by 10 to shift the plot downward. The solid lines are the best fits to the data. The dashed lines are the literature values of the rate constants. (a) Data from the long reactor and (b) data from the short reactor.

ral profile of the CO_2 laser pulse consisted of a narrow peak with a width of about 200 ns, followed by a tail which had significant intensity past 1 μs. So, while some heating took place almost instantaneously, the final temperature in the gas may not have been reached until 1.5 to 2 μs after the front edge of the laser pulse. Therefore, the expansion wave began moving almost instantaneously, but did not reach its final speed until 1.5 to 2 μs after the oscilloscope was triggered by the front edge of the laser pulse. This effect would be independent of the beam diameter, since in all cases heating is complete well before the expansion wave reaches the beam axis. This would therefore result in a uniform upward vertical shift of the delay time vs. beam radius plot and a positive y-intercept, as observed in the short reaction cell. Comparisons of thermal lens signals produced by computer simulations of the experiment verified that noninstantaneous heating resulted in a nearly uniform upward vertical shift in the delay time vs. beam radius plot. Note that this effect would be expected to be the same in both the long and short reaction cells. This effect could be eliminated by shortening the duration of the laser pulse, which can be accomplished by changing the gas mix used in the laser. Unfortunately, doing so substantially decreased the laser energy, such that the temperatures required for reaction could not be obtained with acceptable reaction mixtures.

A second effect that could shift the delay time vs. beam radius plot is due to diffraction of the CO_2 beam by the orifice which defines its diameter. Calculation of Fresnel diffraction patterns shows that in the region just behind the orifice which defines the beam, diffraction leads to an effectively slightly smaller beam diameter and higher intensity near the beam edge. Both radial and axial intensity oscillations may also result. A smaller beam and higher intensity near the beam edge will result in shorter delay times. This shifts the points on the delay time vs. beam radius plot vertically downward. The diffraction pattern is a function of the Fresnel number, $N_f = R^2/(\lambda d)$, where R is the beam radius, λ is the wavelength of the laser, and d is the distance past the orifice [31]. For very large N_f the beam profile is not changed by diffraction. As N_f decreases, the diffraction pattern becomes less uniform, oscillations increase in magnitude, and the effective beam diameter decreases. Thus, for a fixed wavelength, diffraction effects increase with increasing distance past the orifice and decrease with increasing beam diameter. It was experimentally observed that moving the reaction cell further from the orifice decreased the measured delay time, all else remaining constant. Since, on average, the gas in the long cell is further past the orifice than the gas in the short cell, this diffraction effect will be more pronounced in the long reaction cell. This effect can be reduced by using a larger diameter laser beam.

Based on the above, we can attempt to explain the observed delay time vs. beam radius plots. A reasonable hypothesis would be that in the short cell the y-intercept is nonzero due to the finite duration of the laser pulse. In the longer cell, this same effect is present, but is counteracted by the effect of diffraction of the beam such that the y-intercept is nearly zero. We have not yet attempted experiments which could confirm or disprove this hypothesis.

Alternative Treatment of Short Reaction Cell Data

Since the intercept of the delay time vs. beam radius plot for the short reaction cell was nonzero, it would be reasonable to subtract this intercept from the measured delay time before computing the speed of sound. This is equivalent to measuring the delay time starting from a time during the laser pulse rather than from a time at the front edge of it. The effect of making this adjustment is to increase all of the temperature measurements by around 75 K. The Arrhenius plot obtained by making this adjustment is shown in Figure 7. The rate parameters obtained from this plot are shown in Table I. Note that after this adjustment, the absolute values of the rate constants are below the literature values, whereas before the adjustment they were above the literature values. This adjustment results in values for the activation energies which are within 0.3 kcal/mole of the literature values. Adjusting the measured reaction time in this way may help to correct for the effects of noninstantaneous heating in the reactor.

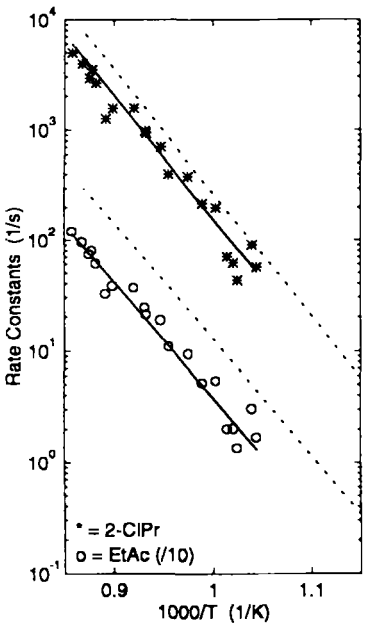

Figure 7 Arrhenius plot of the short reactor data after adjusting the delay time by 0.22 μs. Note that the rate constants for EtAc decomposition have been divided by 10 to shift the plot downward. The solid lines are the best fits to the data. The dashed lines are the literature values of the rate constants.

Comparison of Data in Long and Short Reaction Cells

It was hoped that comparing data between the long and short reaction cells would give us insight into some possible systematic errors in the experiment. These errors would be due to (a) temperature gradients in the axial direction, and (b) diffraction of the beam which heats the gas mixture. In the long reactor, more of the laser energy is absorbed than in the short reactor, and therefore there is a greater temperature difference between the front and the back of the reactor. Also, as discussed above, since the long reactor is, on average, further from the orifice which defines the beam, diffraction effects are more severe. In light of these observations, it is somewhat surprising that the data from the long reactor gives results which are closer to the literature values than does the data from the short reactor. The key difference between the results from the long and short reactors is that slightly higher activation energies are obtained from the long reactor data. It is unclear, however, whether this difference can be attributed to the systematic effects described above. In both reactors, the activation energies are close to those in the literature, so it appears that strong systematic errors were not present in either reactor. The data in the long reactor also has somewhat less scatter. This may be attributed to the fact that the peak in the thermal lens signal from the long reactor is larger, and therefore better measurements of the delay time could be obtained.

Assessing the Accuracy of Temperature Measurements from Thermal Lensing

In order to assess the accuracy and precision of the temperatures measured using the thermal lens technique, one can compare them to temperatures computed from the measured rate constants using the literature values for the activation energies and preexponential factors. Doing so and taking the differences between the temperatures measured from thermal lensing and those calculated from the rate constants gives the results shown in Table II. Since there are some uncertainties in the measured rate constants and in the literature values for the rate parameters, the temperatures calculated here have limited ac-

Table II Differences Between Temperatures from Thermal Lens Signals and Temperatures from Measured Rate Constants

	Long Reaction Cell	Short Reaction Cell	Short Reaction Cell After Adjusting t_r
Mean value of $(T_{TL}-T_{k_{2\text{-ClPr}}})$	5 K	−45 K	32 K
Standard deviation of $(T_{TL}-T_{k_{2\text{-ClPr}}})$	9 K	12 K	14 K
Mean value of $(T_{TL}-T_{k_{EtAc}})$	23 K	−24 K	52 K
Standard deviation of $(T_{TL}-T_{k_{EtAc}})$	9 K	12 K	15 K

T_{TL} = Temperature obtained from thermal lens signal.
$T_{k_{2\text{-ClPr}}}$ = Temperature obtained from the rate constant for 2-ClPr decomposition.
$T_{k_{EtAc}}$ = Temperature obtained from the rate constant for EtAc decomposition.

curacy. However, we can get an idea of the level of uncertainty in the calculated temperatures by looking at the comparative rate data. Because the comparative rate data has much less scatter than the thermal lensing data and gives rate parameters which agree more closely with the literature values, we expect that the temperatures calculated from the measured rate constants will be better estimates of the average reaction temperature than the temperatures from thermal lensing. Thus, they are useful for comparison and evaluation of the accuracy and precision of the thermal lens temperatures. The temperatures measured in the long reactor using thermal lensing agree well with the temperatures from the rate constants. The average difference between the temperature from the thermal lens signal and the temperature calculated from the 2-ClPr rate constant is only 5 K. The standard deviation of this temperature difference is about 9 K. This means that about 70% of the thermal lens temperatures lie in the range from 4 degrees below to 14 degrees above the temperature calculated from the 2-ClPr rate constant. The interpretation of the other numbers in Table II is analogous. We may therefore conclude from Table II that in the long reactor, we are successful in measuring absolute values of temperature to within ± 20 K and relative temperatures to within ± 10 K. In the short reactor, with either method of data analysis, absolute temperatures are within ± 50 K and relative temperatures are within ± 15 K. By relative temperatures, we mean differences between pairs of temperatures measured by thermal lensing (in the same reactor). Note that errors in absolute temperature measurement predominantly affect the preexponential factor while errors in relative temperatures predominantly affect the activation energy.

Consideration of Other Possible Systematic Errors in the Experiment

Two recognizable sources of systematic error in the rate constant determinations which have not been explicitly mentioned so far are (1) errors due to the noninstantaneous heating of the gas mixture, and (2) errors due to nonuniformity of the laser energy. These were explored using computational simulations of the experiment for conditions close to those actually used. When heating of the reactant gas is not instantaneous, the rarefaction wave starts to move before the gas reaches the final reaction temperature. Therefore, a smaller volume of gas reaches the final temperature and less reaction occurs. However, since the rarefaction wave does not achieve its final velocity immediately, it also takes longer for it to reach the axis than it would if heating had been instantaneous, and the measured delay time is increased. This means that the measured temperature will be lower than the actual reaction temperature. These two effects clearly work in opposite directions, the first leading to a low value for the rate constant and the second leading to a high value (through a low temperature measurement). Computational simulations of the experiment reveal that, for the reactor conditions used in these experiments, the second effect dominates. With the noninstantaneous heating somewhat exaggerated, the simulation gave rate constants which were about 70% high and an activation energy that was almost 1 kcal/mole low. For the actual laser pulse shape in the experiment, the effect should have been smaller.

Nonuniformity of the spatial energy profile of the CO_2 laser has a similar effect to noninstantaneous heating. The portion of the laser beam used in these experiments had a profile that was almost uniform in the horizontal direction, but decreased in energy in the vertical direction moving away from the beam axis. At the top and bottom edge of the 0.635 cm diameter portion of the beam used here, the laser intensity was about 15% lower than on the beam axis. The temperature profile would be expected to be qualitatively similar, but we expect that saturation of the photosensitizer leads to some smoothing of the temperature profile. With this in mind, computer simula-

tions were performed for a worst case scenario in which the temperature profile was uniform horizontally and decreased linearly in the vertical direction, such that the temperature rise at the top edge of the beam was only 80% of the temperature rise at the center. Only one quarter of the reactor was simulated, since the temperature profile had horizontal and vertical planes of symmetry. Results were compared to simulations in which heating was uniform. The lower average temperature results in less reaction than if heating was uniform (for the same temperature at the center of the reactor). However, the lower average temperature also leads to a longer delay time, and therefore a lower temperature obtained from the thermal lens signal. As with noninstantaneous heating, these two effects work in opposite directions, and the net result is the same. The lower measured temperature dominates so that the rate constants obtained are high. For the worst case scenario simulated, they were high by about a factor of 3 and the activation energy was low by almost 1.5 kcal/mole.

The two potential sources of systematic error discussed above could account for the results obtained in the short reactor. In Figure 6(b), we see that the measured values of the rate constants are consistently above the literature values and the activation energies obtained from the data are slightly below the literature values. This is qualitatively what one would expect based on the numerical simulations. However, that does not explain why the data from the long reactor does not show these effects. Experiments to investigate this directly would require adjusting the spatial uniformity and pulse duration of the laser independently of each other and independently of the laser energy. This is not feasible.

Potential Improvements in the Technique

The key to improving temperature measurements and the resulting rate parameter determinations is improvement of the laser used to heat the reaction mixture. A higher power laser would allow the use of a shorter laser pulse duration and would decrease axial temperature gradients. It would also allow work at higher pressures, since more energy would be available to heat the gas. A larger usable beam diameter would decrease the effects of beam diffraction by the orifice which defines it and would increase the reaction time. Increasing the total reaction time decreases the relative error in the time measurement, since the absolute uncertainty in the time measurement is nearly constant. A more uniform beam would eliminate possible systematic error due to temperature nonuniformities in the plane perpendicular to the reactor axis. For these reasons, the laser used in the experiment seems to be the most important factor in improving this technique.

CONCLUSION

The key conclusion to be drawn from this work is that pulsed LPHP with temperature measurement from thermal lens signals, as presented here, can provide useful measurements of rate parameters for unimolecular decomposition reactions. We were successful in determining the absolute values of rate constants to within a factor of 3 and activation energies to within 4 kcal/mole of the literature values in both reactors used and for both reactions investigated here. For the best results (2-ClPr decomposition in the long reactor) all of the data points were within 40% of the recommended values of the rate constant. The best fit line was within 4% of the literature values over the temperature range of the experiments. This is less than the uncertainty in the recommended values. Average absolute temperatures in these experiments agreed with the temperatures calculated from the measured rate constants to within ± 20 K in the long reactor, where the best results were obtained. In this same reactor, relative temperatures were measured to within ± 10 K. Some potential sources of the remaining error in the temperature measurement have been explored and discussed.

Using the comparative rate technique, activation energies can be determined to within 0.5 to 1 kcal/mole, provided there is negligible uncertainty in the rate parameters of the reference reaction. Experiments where temperatures are determined from thermal lensing can be used to check the results of comparative rate studies to ensure that the presence of the thermal monitor molecule does not affect the rate of the reaction under consideration. Rate parameters (of limited accuracy) may be obtained using thermal lensing to measure the temperature in mixtures not containing the thermal monitor molecule. These values can be compared to the results from comparative rate experiments. If there are significant differences, then we can conclude that the thermal monitor interferes with the reaction under consideration. If not, then we can accept with confidence the more accurate measurements from the comparative rate experiments. So the method of temperature measurement described here can be useful alone in providing coarse measurements of rate parameters and can be useful in conjunction with comparative rate experiments in providing more accurate measurements.

Support in the form of a graduate fellowship from the National Science Foundation and a Doctoral Dissertation Fellowship from the University of Minnesota is gratefully acknowledged. We would also like to thank Ryan Fujimoto for valuable technical assistance on this project.

BIBLIOGRAPHY

1. D. K. Russell, *Chem. Soc. Rev.*, **19,** 407 (1990).
2. D. F. McMillen, K. E. Lewis, G. P. Smith, and D. M. Golden, *J. Phys. Chem.*, **86,** 709 (1982).
3. H. L. Dai, E. Specht, M. R. Berman, and C. B. Moore, *J. Chem. Phys.*, **77,** 4494 (1982).
4. C. Steel, V. Starov, R. Leo, P. John, and R. G. Harrison, *Chem. Phys. Lett.*, **62,** 121 (1979).
5. K. E. Lewis, D. M. Golden, and G. P. Smith, *J. Am. Chem. Soc.*, **106,** 3905 (1984).
6. K. L. Knutson, R. W. Carr, W. H. Liu, and S. A. Campbell, *J. Crystal Growth*, **140,** 191 (1994).
7. M. Hierlemann, A. Kersch, C. Werner, and H. Schäfer, *J. Electrochem. Soc.*, **142,** 259 (1995).
8. T. J. Mountziaris and K. F. Jensen, *J. Electrochem. Soc.*, **138,** 2426 (1991).
9. M. E. Coltrin, R. J. Kee, and J. A. Miller, *J. Electrochem. Soc.*, **133,** 1206 (1986).
10. M. E. Coltrin, R. J. Kee, and J. A. Miller, *J. Electrochem. Soc.*, **131,** 425 (1984).
11. J. R. Guckert and R. W. Carr, *J. Phys. Chem.*, **90,** 4286 (1986).
12. P. M. Kuchibhotla, *PhD Thesis*, University of Minnesota, 1989.
13. J. R. Barker and T. Rothem, *Chem. Phys.*, **68,** 331 (1982).
14. R. T. Bailey, F. R. Cruickshank, R. Guthrie, D. Pugh, and I. J. M. Weir, *Mol. Phys.*, **48,** 81 (1983).
15. M. T. Swihart and R. W. Carr, *Int. J. Chem. Kinet.*, **26,** 779 (1994).
16. H. Heydtmann, B. Dill, and R. Jonas, *Int. J. Chem. Kinet.*, **7,** 973 (1975).
17. P. Cadman, M. Day, and A. F. Trotman-Dickenson, *J. Chem. Soc. (A)*, 2498 (1970).
18. W. Tsang, *J. Chem. Phys.*, **41,** 2487 (1964).
19. K. E. Howlett, *J. Chem. Soc.*, 3695 (1952).
20. D. H. R. Barton and A. J. Head, *Trans. Faraday Soc.*, **46,** 114 (1950).
21. S. Norfolk and R. Taylor, *J. Chem. Soc. Perkin II*, 280 (1976).
22. R. Taylor, *J. Chem. Soc. Perkin II*, 1025 (1975).
23. P. C. Beadle, D. M. Golden, and S. W. Benson, *Int. J. Chem. Kinet.*, **4,** 265 (1972).
24. J. C. Scheer, E. C. Kooyman, and F. L. J. Sixma, *Rec. Trav. Chim. des Pays-Bas*, **82,** 1123 (1963).
25. A. T. Blades and P. W. Gilderson, *Can. J. Chem.*, **38,** 1407 (1960).
26. A. T. Blades, *Can. J. Chem.*, **32,** 366 (1954).
27. S. W. Benson and H. E. O'Neal, *Kinetic Data on Gas Phase Unimolecular Reactions*, U. S. Department of Commerce National Bureau of Standards Report NRSDS-NBS 21, 1970.
28. M. W. Chase, Jr., C. A. Davies, J. R. Downey, Jr., D. J. Frurip, R. A. McDonald, and A. N. Syverud, *J. Phys. Chem. Ref. Data*, **14,** supplement no. 1, (1985).
29. T. E. Daubert and R. P. Danner, *Physical and Thermodynamic Properties of Pure Chemicals: Data Compilation*, Taylor and Francis, 1993.
30. W. Tsang, *J. Chem. Phys.*, **40,** 1171 (1964).
31. B. E. A. Saleh and M. C. Teich, *Photonics*, Wiley-Interscience, 1991, pp. 131–134.